



Research article

Low protein expression of LZTR1 in hepatocellular carcinoma triggers tumorigenesis *via* activating the RAS/RAF/MEK/ERK signaling

Ganghui Ye^{a,b,1}, Jie Wang^{a,b,1}, Jingyi Xia^c, Chenlu Zhu^c, Chaoyu Gu^b,
Xinming Li^b, Jingyun Li^{a,b}, Meng Ye^{a,b,**}, Xiaofeng Jin^{a,b,*}

^a Department of Biochemistry and Molecular Biology, Health Science Center, Ningbo University, Ningbo, 315211, China

^b Department of Oncology, The First Hospital of Ningbo University, Ningbo, 315020, China

^c Zhejiang Key Laboratory of Pathophysiology, Department of Biochemistry and Molecular Biology, Health Science Center of Ningbo University, Ningbo, 315211, China

ARTICLE INFO

Keywords:

LZTR1
Hepatocellular carcinoma
KRAS
Degradation
Lenvatinib
Drug resistance

ABSTRACT

LZTR1 is a substrate specific adaptor for E3 ligase involved in the ubiquitination and degradation of RAS GTPases, which inhibits the RAS/RAF/MEK/ERK signaling to suppress the pathogenesis of Noonan syndrome and glioblastoma. However, it's still unknown whether LZTR1 destabilizes RAS GTPases to suppress HCC progression by inhibiting these signaling pathway. Lenvatinib is the first-line drug for the treatment of advanced HCC, however, it has high drug resistance. To explore the roles of LZTR1 in HCC progression and the underlying mechanisms of lenvatinib resistance, techniques such as bioinformatics analysis, immunohistochemical staining, RT-qPCR, Western blot, cell functional experiments, small interfering RNA transfection and cycloheximide chase assay were applied in our study. Among these, bioinformatics analysis and immunohistochemical staining results indicated that LZTR1 protein was aberrantly expressed at low levels in HCC tissues, and low protein expression of LZTR1 was associated with poor prognosis of HCC patients. *In vitro* functional experiments confirmed that low expression of LZTR1 promoted HCC cell proliferation and migration *via* the aberrant activation of the RAS/RAF/MEK/ERK signaling due to the dysregulation of LZTR1-induced KRAS ubiquitination and degradation. Transwell assays revealed that blocking of LZTR1-mediated KRAS degradation could induce lenvatinib resistance in HCC cells. In conclusion, our study revealed that LZTR1 knockdown promoted HCC cell proliferation and migration, and induced lenvatinib resistance *via* activating the RAS/RAF/MEK/ERK signaling, which may provide new ideas for HCC treatment.

1. Introduction

Primary liver cancer is the sixth most common cancer and the third leading cause of cancer-related death worldwide, and the number of death due to liver cancer is as high as 830,000 in 2020 [1]. Even with the advancement of medical technology and sanitation

* Corresponding author. Department of Biochemistry and Molecular Biology, Health Science Center, Ningbo University, Ningbo, 315211, China.

** Corresponding author. Department of Biochemistry and Molecular Biology, Health Science Center, Ningbo University, Ningbo, 315211, China.

E-mail addresses: yemeng@nbu.edu.cn (M. Ye), jinxiaofeng@nbu.edu.cn (X. Jin).

¹ Contributed equally.

<https://doi.org/10.1016/j.heliyon.2024.e32855>

Received 24 April 2023; Received in revised form 10 June 2024; Accepted 11 June 2024

Available online 14 June 2024

2405-8440/© 2024 The Authors. Published by Elsevier Ltd. This is an open access article under the CC BY-NC-ND license (<http://creativecommons.org/licenses/by-nc-nd/4.0/>).

conditions, the incidence and death rate of liver cancer remain high, and the prognosis is still poor. Hepatocellular carcinoma (HCC) is the most common type of liver cancer and accounts for approximately about 80 % of all primary liver cancers. In contrast to the high mortality rate, the detection rate of HCC is very low, and more than 90 % of early HCCs are found to be at an advanced stage with a low 5-year survival rate (approximately 10 %) [2]. Recently, despite the advantages of targeted treatment and immunotherapy [3,4], the treatment of HCC patients still faces many major challenges such as drug resistance, individualized differences and severe side effects. Thus, an attempt to discover associated underlying mechanism, novel therapeutic targets, better diagnostics and promising biomarkers is still urgently needed.

Multiple intracellular signaling pathways, including the Wnt signaling [5], the mammalian target of rapamycin (mTOR) pathway [6], the Hippo signaling and the mitogen-activated protein kinase (MAPK) pathway [7], are involved in the occurrence and progression of HCC and are closely related to therapeutic choices and outcomes. The RAS/RAF/MEK/ERK pathway is one of the primary MAPK signaling cascades involved in regulating cell proliferation, differentiation, apoptosis and stress response [8] and plays crucial roles in the occurrence and progression of multiple cancer types, including colon cancer [9], HCC [10], leukemia [11], and melanoma [12]. The RAS which shown are small GTPases that are activated in response to a series of external stimuli. In RAS/RAF/MEK/ERK signaling, activated RAS protein induces dimerization and activation of RAF, which then phosphorylates and activates MEK, leading to the phosphorylation and activation of ERK [13]. Phosphorylated-ERK (P-ERK), the active form of ERK, is a significant indicator of RAS/RAF/MEK/ERK signaling activity [14]. Mutations in RAS gene account for approximately 30 % of all cancers [15] and are frequently responsible for RAS overactivation in human cancer [16,17]. In HCC tissues, aberrant activation of this pathway has been widely reported and proven to be closely related to HCC occurrence, malignant transformation [18] and drug resistance [19]. Conversely, unlike the extensive activation of this signaling, RAS mutations are rarely found, and are detected in less than 5 % of HCC cases [20], which triggers the contemplation of whether other uncovered mechanisms are involved in the overactivation of this pathway.

Ubiquitination is an important post-translational modification (PTM), that influences the fates of almost all cellular proteins and participates in regulating a variety of physiological cellular functions [21]. Dysregulation of ubiquitination is closely associated with the occurrence and progression of a wide range of tumor types [22], including HCC [23]. Leucine zipper-like transcription regulator 1 (LZTR1), a member of the BTB-Kelch protein family, is a substrate specific adaptor for the Cullin3-RING E3 ligase (CRL3) ubiquitin ligase complex that regulates a range of cell pathophysiological functions [24]. LZTR1 is regarded as a tumor suppressor gene, and its mutations are closely associated with the pathogenesis of Noonan syndrome (NS), glioblastoma and chronic myeloid leukemia [25]. In recent years, several studies have found that LZTR1 could induce RAS protein ubiquitination and degradation to inhibit the RAS/RAF/MEK/ERK signaling pathway [26,27], which was also confirmed in pancreatic cancer [28] and melanoma [29]. To date, it remains unknown whether LZTR1 participates in regulating this signaling *via* mediating RAS protein ubiquitination and degradation to affect HCC occurrence and progression. Herein, we detected LZTR1 expression at low protein levels in HCC tissues compared to that in adjacent normal tissues using immunohistochemistry (IHC). Through bioinformatic analysis, no difference was observed in the transcript levels of LZTR1 between HCC and adjacent normal tissues. Conversely, the LZTR1 protein was found to be weakly expressed in HCC tissues, and high LZTR1 protein levels were significantly associated with good prognosis. Furthermore, through *in vitro* functional experiments, we found that low expression of LZTR1 facilitated the proliferation and migration of HCC cells *via* activating the RAS/RAF/MEK/ERK signaling. Furthermore, low expression of LZTR1 results in resistance to lenvatinib in HCC cell lines, which partly indicates the relationship between low protein expression of LZTR1 and worse outcomes in HCC patients.

2. Materials and methods

2.1. Antibodies and reagents

The following main antibodies and reagents were utilized: LZTR1 Rabbit pAb (A7350, Abclonal, Wuhan, China), ERK1/2 Rabbit mAb (A4782, Abclonal, Wuhan, China), KRAS Rabbit pAb (12063-1-AP, Proteintech, Wuhan, China), KRAS + HRAS + NRAS Rabbit mAb (A19779, Abclonal, Wuhan, China), Phospho-ERK-T202/204 + ERK2-T185/Y187 Rabbit pAb (AP0472, Abclonal, Wuhan, China), GAPDH Rabbit pAb (AC001, Abclonal, Wuhan, China), and HRP Goat Anti-Rabbit IgG (AS014, Abclonal, Wuhan, China), HA Rabbit pAb (51064-2-AP, Proteintech, Wuhan, China), Myc Rabbit pAb (16286-1-AP, Proteintech, Wuhan, China) and Flag Rabbit pAb (20543-1-AP, Wuhan, China).

2.2. Ethics statement

All human samples were obtained after obtaining informed consent from patients. Ethics approval and consent for the use of human tissue were obtained from the ethics committee of the Health Science Center, Ningbo University with the approval number: NBU-2021-121, dated July 10, 2021.

2.3. Patients and tissue samples

The 76 patients included in our study were diagnosed as HCC and confirmed by histology in the Ningbo Clinicopathological Diagnosis Center from January 1, 2021, to July 31, 2022. After, the ethics statement has been approved (July 10, 2021), we start to collect these HCC specimens, including 44 pairs of formalin-fixed human HCC tissue samples and 32 pairs fresh of human HCC samples. The clinicopathological characteristics for 76 patients including age, gender, tumor number, tumor size, liver cirrhosis, HBV-affected,

differentiation, microvascular invasion, liver capsule invasion, AFP level and TNM stage, were retrospectively collected. After fully being introduced the research purpose, all participants understood the research-use of human tissues, their rights, the potential risks and benefits of this research, and agreed to join the study. Due to some patients' concerns about privacy of written signatures and the protection of patient information, we obtain verbal consent from each participant. The staining intensities of HCC and paired adjacent normal tissues are shown in Table 1. The specific clinical information is shown in Fig. 1H and Table 2.

2.4. Immunohistochemical staining

HCC tissues were placed in embedding cassettes, fixed with 4 % paraformaldehyde for 24 h, and dehydrated with 75 % ethanol for 1 h, 85 % ethanol for 1 h, 95 % ethanol thrice for 1 h, anhydrous ethanol twice for 1 h, and xylene solution twice for 40 min. Next, dehydrated tissues were embedded in melted paraffin (Sinopharm Chemical Reagent Co., Ltd) three times for 1 h. Paraffin-embedded tissues were cut into 4 μ m sections using a rotary microtome (Leica microtome; Leica), and sections were roasted in an oven at 60 °C for 3 h. Then, high quality roasted tissue sections were deparaffinized with xylene twice for 10 min, rehydrated with anhydrous ethanol twice for 5 min, 95 % ethanol for 5 min, 85 % ethanol for 5 min, 75 % ethanol for 5 min, deionized water for 5 min. Next, tissue sections were placed in repair boxes filled with Ethylene Diamine Tetraacetic Acid (EDTA) antigen repair buffer, PH8.0 (P0085, Beyotime, Shanghai, China), underwent high-pressure antigen repairing for 8 min, permeabilized using 0.5 % Triton X-100 (T8200, Solarbio, Beijing, China) for 20 min, blocked with 3 % hydrogen peroxide for 10 min and 10 % goat serum (SL038, Solarbio, Beijing, China) for 15 min, and incubated with LZTR1 antibody (A7350, Abclonal, Wuhan, China) (1:100) at 4 °C overnight. The following day, secondary antibodies (AS014, Abclonal, Wuhan, China) (1:2000) were incubated at room temperature for 1 h and DAB kits (G1212, Solarbio, Beijing, China) were used for staining for 1 min. Hematoxylin (G4070, Solarbio, Beijing, China) was used to stain the nucleus for 45 s.

Immunohistochemical staining was evaluated by two independent pathologists. Staining intensity grades were divided into three group: negative, low positive and high positive and were scored as 0, 1 and 2, respectively. Staining positive cell rates and its corresponding scores were classified as follow: 0, <10 %; 1, 10–50 %; and 2, >50 %. The final IHC scores were calculated as the sum of the staining intensity scores and staining positive cell rate scores.

2.5. Analysis of LZTR1 mRNA expression in HCC tissues and normal liver tissues from the genotype-tissue expression project and the cancer genome atlas databases

The RNA-seq data (FPKM value) of LZTR1 in HCC tissues and normal liver tissues (adjacent normal tissues and healthy liver tissues) were downloaded from the Genotype-Tissue Expression (GTEx) project (<https://xenabrowser.net/datapages/>) and the Cancer Genome Atlas (TCGA) databases (<https://portal.gdc.cancer.gov/>). The FPKM values were transformed to Log₂ (FPKM+1). And the analysis of LZTR1 mRNA expression in HCC tissues and normal tissues was conducted by the “BioManager”, “limma”, “ggplot2” packages in R software.

2.6. Analysis of LZTR1 protein expression in HCC tissues and adjacent normal tissues, and correlation between LZTR1 expression and prognosis in HCC patients from the Clinical Proteomic Tumor Analysis Consortium Data Portal

Raw proteomic data of LZTR1 in HCC tissues and adjacent normal tissues were downloaded from the Clinical Proteomic Tumor Analysis Consortium (CPTAC) Data Portal (<https://pdc.cancer.gov/pdc/>). The z-scores in the raw proteomic data were used to represent protein expression. The z-scores were transformed to Log₂ (z-score+1). Analysis of LZTR1 protein expression in HCC tissues and adjacent normal tissues was conducted by the “BioManager”, “limma”, “ggplot2” packages in R software. Survival analysis were performed by the “survival”, “Survminer” packages in R software. Heatmaps of clinicopathologic characteristics in different LZTR1 protein expression groups were created with the “ComplexHeatmap” package in R software.

2.7. Cell culture

Human HCC cell lines HepG2, SK-Hep1, Hep3B and PLC/PRF/5 were obtained from the American Type Culture Collection (ATCC), which were cultured with Dulbecco's Modified Eagle Medium (DMEM) supplemented with 10 % fetal bovine serum (FBS) and 1 % penicillin-streptomycin. Human HCC cell line JHH1 was obtained from the Japanese Collection of Research Bioresources (JCRB), which was cultured in William's E Medium (WEM) with 10 % FBS and 1 % penicillin-streptomycin. All cells were grown in a 37 °C CO₂ humidity incubator with 5 % CO₂. The fresh cell medium was replaced every 1–2 days to maintain normal cell growth.

Table 1

Comparisons with immunohistochemical staining intensity of LZTR1 between HCC and paired adjacent normal tissues.

| Number | LZTR1 level | | | χ^2 | P value |
|--------|-------------|--------------|---------------|-------------|---------|
| | Negative | Low Positive | High Positive | | |
| Tumor | 76 | 40 (52.6 %) | 27 (35.5 %) | 9 (11.9 %) | <0.001 |
| Normal | 76 | 12 (15.8 %) | 40 (52.6 %) | 24 (31.6 %) | |

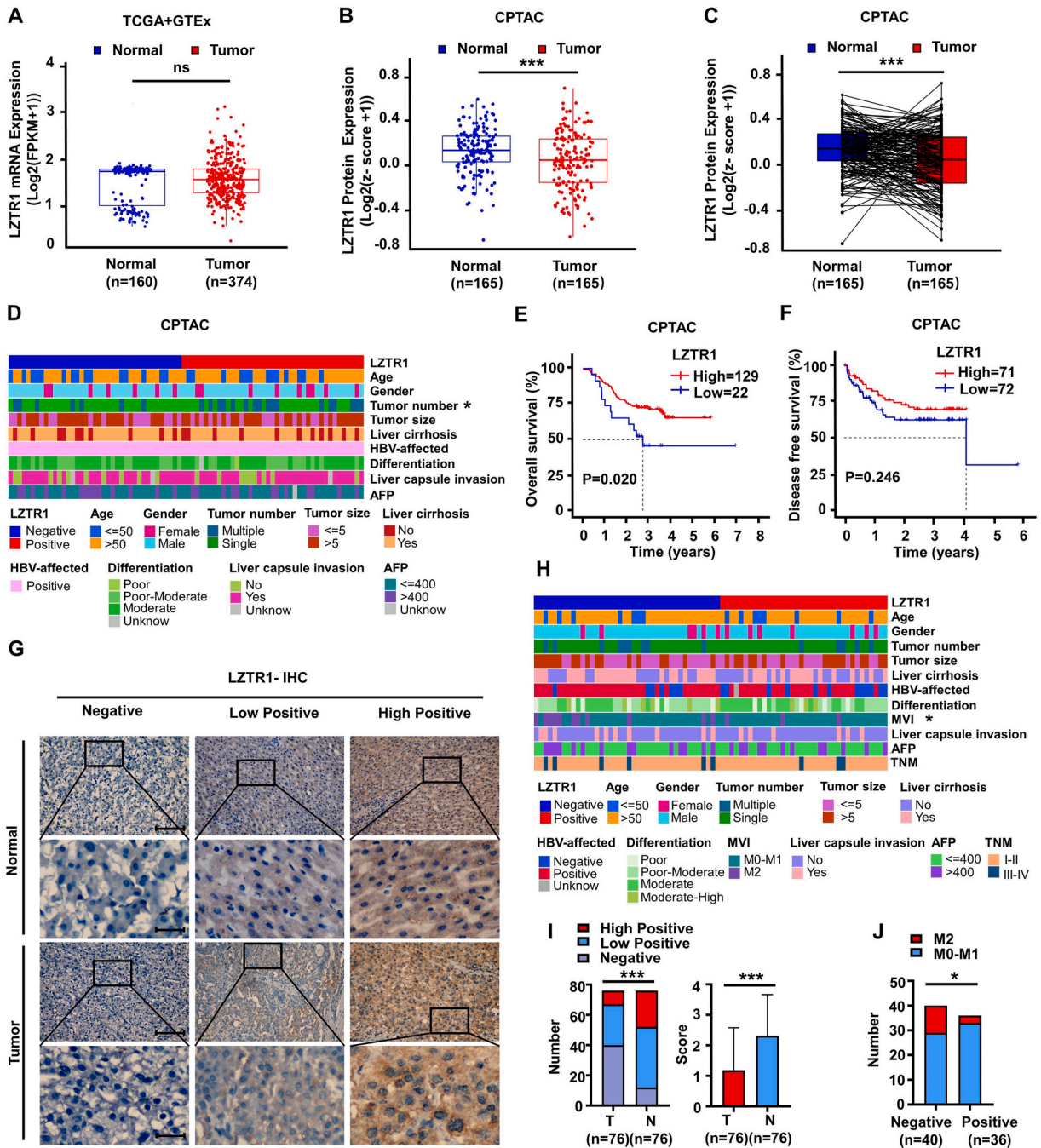


Fig. 1. Low expression of LZTR1 is related to the worse outcome of HCC patients. **A** Differential expression analysis of *LZTR1* mRNA levels in HCC tissues and adjacent normal tissues from TCGA and GTEx database using R software. **B–C** Differential expression analysis of *LZTR1* protein levels in 165 paired HCC tissues and adjacent normal tissues from CPTAC database using R software. **D** A heatmap depicting the relationship between the clinicopathological characteristics and *LZTR1* expression from CPTAC database using R software. **E** Association between *LZTR1* protein expression and overall survival in HCC patients from CPTAC database using R software. **F** Association between *LZTR1* protein expression and disease-free survival in HCC patients from CPTAC database using R software. **G** Representative immunohistochemical images for *LZTR1* expression in HCC tissues (T) and paired adjacent normal tissues (N). Based on staining intensity standards, results of immunohistochemical staining were divided into negative, low positive and high positive. Scale bar, 100 μ m (upper) and 25 μ m (below). **H** A heatmap depicting the relationship between the clinicopathological characteristics and *LZTR1* expression using R software. **I** Results of IHC staining intensity and staining score were shown as column charts. **J** Results of microvascular invasion grades of patients in negative and positive staining groups were shown as column charts. Asterisk represents the significant difference. * $P < 0.05$, ** $P < 0.01$, *** $P < 0.001$.

Table 2
Correlation between the clinicopathological characteristics and LZTR1 protein expression in HCC.

| Variable | Number | LZTR1 level | | χ^2 | P value |
|------------------------|--------|---------------|---------------|----------|--------------|
| | | Negative (40) | Positive (36) | | |
| Age (years) | | | | | |
| ≤50 | 14 | 7 | 7 | 0.048 | 0.827 |
| >50 | 62 | 33 | 29 | | |
| Gender | | | | | |
| Male | 63 | 34 | 29 | 0.264 | 0.607 |
| Female | 13 | 6 | 7 | | |
| Tumor number | | | | | |
| Single | 62 | 31 | 31 | 0.064 | 0.801 |
| Multiple | 14 | 9 | 5 | | |
| Tumor size (cm) | | | | | |
| ≤5 cm | 41 | 23 | 18 | 0.429 | 0.512 |
| >5 cm | 35 | 17 | 18 | | |
| Liver cirrhosis | | | | | |
| Yes | 41 | 24 | 17 | 1.245 | 0.264 |
| No | 35 | 16 | 19 | | |
| HBV-affected | | | | | |
| Negative | 19 | 7 | 12 | 2.781 | 0.095 |
| Positive | 56 | 33 | 23 | | |
| Differentiation | | | | | |
| Poor | 12 | 7 | 5 | 3.294 | 0.354 |
| Poor-Moderate | 27 | 16 | 11 | | |
| Moderate | 28 | 11 | 17 | | |
| Moderate-High | 9 | 6 | 3 | | |
| Microvascular invasion | | | | | |
| M0-M1 | 62 | 29 | 33 | 4.632 | 0.031 |
| M2 | 14 | 11 | 3 | | |
| Liver capsule invasion | | | | | |
| Yes | 16 | 10 | 6 | 0.792 | 0.374 |
| No | 60 | 30 | 30 | | |
| AFP level (ng/L) | | | | | |
| ≤400 | 50 | 26 | 24 | 0.023 | 0.878 |
| >400 | 26 | 14 | 12 | | |
| TNM stage | | | | | |
| I-II | 67 | 34 | 33 | 0.063 | 0.802 |
| III-IV | 9 | 6 | 3 | | |

Negative: Negative expression of LZTR1. Positive: Positive expression of LZTR1.

2.8. Screening of stable expression HCC cell lines

Using the CRISPR online design tools CRISPR direct (<https://crispr.dbcls.jp/>). A single guide (sg) RNA target site (5'-AGTCTTT-CACATCGAACCGC-3') was identified in the coding region of LZTR1 gene. The pCDH-CMV-MCS-EF1-CopGFP-T2A-Puro (CD513B)-empty plasmid, CD513B-LZTR1 overexpression plasmid and CD513B-CRISPR-cas9-LZTR1 plasmid were constructed by GenePharma (Shanghai, China). HepG2 and SK-Hep1 cells were transfected with CD513B-empty plasmid, CD513B-LZTR1 overexpression plasmid and CD513B-CRISPR-cas9-LZTR1 plasmid using the Lipo8000 Transfection Reagent (C0533, Beyotime, Shanghai, China) according to the manufacturer's instructions. 48 h after transfection, the cell culture medium was discarded and cells were washed twice with PBS. Subsequently, culture medium containing 2 µg/ml puromycin (**Supplementary file 1-Fig. 3**) was added and the cell culture was continued for 24 h. After 24 h, the culture medium (2 µg/ml puromycin) was changed, followed by medium changes every 2–3 days. The GFP fluorescence intensity was observed with a fluorescence microscope every 2–3 days, and the normal medium was replaced when the field was full of fluorescent cells. However, it has been theorized that the LZTR1-knockout cell lines should be generated using CRISPR-Cas9 methods in HCC cells. In our experiments, the mRNA and protein expression of LZTR1 can still be detected in HCC screened cells due to the suboptimal efficiency of puromycin screening method. Therefore, the term "LZTR1-knockdown" was used in our paper. The mRNA and protein expression levels of LZTR1 in cells were determined using real-time reverse transcription polymerase chain reaction (RT-qPCR) and Western blot, respectively.

2.9. Small interfering RNA transfection

The small interfering RNA (siRNA) was purchased from Tsingke Biotechnology Co., Ltd. (Hangzhou, China). The following sequences used were as follows: siKRAS-1 sense: 5'-CACCAUUAUAGAACAAA (dT) (dT)-3' and antisense 5'-UUUGUUCUCUAUAAUGGUG (dT) (dT)-3'. siKRAS-2 sense: 5'-GAAGUUAUGGAAUUCUUU(dT) (dT)-3' and antisense 5'-AAAGGAAUUCUAACUUC(dT) (dT)-3'. siKRAS-3 sense: 5'-CUUCUAUACAUAUAGUUCGA(dT) (dT)-3' and antisense 5'-UCGACUAAUGUAUAGAAG (dT) (dT)-3'. The siKRAS-3 was chosen to conduct the following experiments for its relatively higher knockdown efficiency (as described in **Fig. 5B–C**). The siRNA

transfection was performed using Lipo8000 Transfection Reagent according to the manufacturer's instructions. The following experiments were conducted 48 h after siRNA transfection.

2.10. Real-time reverse transcription polymerase chain reaction

Total RNA was isolated from HepG2 and SK-Hep1 cells using TRIzol reagent (Tiangen, China), and cDNA was reverse transcribed using the HiScript® II 1st Strand cDNA Synthesis Kit (Vazyme, Nanjing, China) according to the manufacturer's instructions. PCR amplification was performed using the SYBR Green PCR Master Mix Kit (Vazyme, Nanjing, China) according to the manufacturer's instructions. The PCR primers were also purchased from Tsingke Biotechnology Co., Ltd. The primer sequences for PCR were as follows (5'-3', sense, antisense), *LZTR1* forward: 5'-GCGGGGAGATGTACAAGTT-3' and reverse: 5'-CCCCTAGTCCTCGTGCA-3', *KRAS* forward: 5'-AGTCATGGTCACTCTCCCA-3' and reverse: 5'-GCAGTCTGACACAGGGAGAC-3', *GAPDH* forward: 5'-CCCTCATGCCTGCTTC-3' and reverse: 5'-CATGCCTTCCTGTTCC-3'.

2.11. Western blot analysis

HepG2 and SK-Hep1 cells were washed twice with PBS and lysed in RIPA (high) lysis buffer containing 1 % phenylmethanesulfonyl fluoride (ST-506, Beyotime, Shanghai, China) and 2 % phosphatase inhibitor cocktail A (P1081, Beyotime, Shanghai, China). Samples were centrifuged at 4 °C, 12,000 rpm for 20 min, mixed with 4 × sodium dodecyl sulfate (SDS) and heated for 5 min in a 97 °C metal bath. Mixed protein extracts were subjected to SDS-PAGE electrophoresis, and transferred to hydrophobic polyvinylidene fluoride (PVDF) membranes (GE Healthcare Sciences). Then, membranes were blocked with 5 % skim milk powder in TBST for 45 min, washed with TBST twice for 5 min, and incubated with primary antibodies on a 4 °C shaker overnight. After overnight incubation, membranes were washed with TBST five times for 5 min, incubated with the corresponding secondary antibodies on a 4 °C shaker for 1 h and washed five times again. Finally, the results were visualized using ECL reagent (Santa Cruz Biotechnology) and X-ray film exposure. The experiments were performed 2–3 times and the representative images were shown.

2.12. Cell proliferation assay

HepG2 and SK-Hep1 cell proliferation was measured via the Cell Counting Kit 8 (CCK8) assay (K1018, Apexbio, America) according to the manufacturer's instructions. Control, overexpression and knockdown groups-LZTR1 HCC cells were selected and seeded into 96-well plates with 1.5×10^3 cells per well. And, each well was added with a total of 10 μ L CCK8 solution, and the cells in wells were incubated for 2 h. The absorbance values at 450 nm were measured using a micro plate reader (Thermo Fisher Scientific, Inc.) at 0, 24, 48, 72, 96, 120 and 144 h, which were also utilized to represent cell proliferation rates in different groups. The results were analyzed using GraphPad Prism 8.

2.13. Colony formation assay

HepG2 and SK-Hep1 cells were seeded in 6-well plates at a density of 1500 cells per well (three wells per group). The fresh medium was changed every 3–4 days. After two weeks of incubation, culture medium was discarded and cells were washed once with PBS, fixed with ice-cold methanol for 10 min at 4 °C, and washed with PBS again. Then, cells were stained with crystal violet solution (G4070, Solarbio, Beijing, China) for 20 min on a shaker. The images of cell colonies were captured using a scanner (CanoScan LiDE 300, Canon) and analyzed using Image J software.

2.14. Transwell migration assay

HepG2 and SK-Hep1 cell migration was detected using transwell assays (8.0 μ m, 3342, Corning, USA). Cells were starved in culture medium with free serum for 24 h and seeded onto transwell chambers with 4×10^4 cells per chamber. Cells were allowed to migrate towards the bottom wells. After 24 h of incubation, transwell membranes were washed twice with PBS, fixed with iced methanol for 10 min at 4 °C, and washed with PBS again. The cells on the membranes were then stained with crystal violet solution for 20 min on a shaker. Four randomly selected fields on each transwell membrane were photographed with 100-fold magnification using an inverted optical microscope and analyzed using Image J software.

2.15. Wound healing migration assay

HepG2 and SK-Hep1 cells were seeded in 6-well plates (three horizontal lines were drawn in advance on the plate back) with 3×10^5 cells per well (two wells in each group). After the degree of cell fusion reached 80–90 %, 5 μ g/ml mitomycin C (M5353, Sigma, Shanghai, China) was used for 12 h to inhibit cell division. After the pretreatment process, 10 μ L gun heads were used to draw three lines perpendicular to the horizontal lines per well. PBS were used to wash gently floating cells twice, and the culture medium containing 2 % serum was replaced to remove the effect of cell proliferation. The pictures of wound healing at 0 and 24 h were observed under an inverted microscope and scratch areas were calculated using the Image J software. Cell migration rates = (0-h scratch area – 24-h scratch area)/(0-h scratch area) × 100 %.

2.16. Half maximal inhibitory concentration assay

HepG2 cells were used for the half maximal inhibitory concentration (IC₅₀) assay. HepG2 cells were seeded in 96-well plates at a density of 5000 cells per well and were cultured overnight. Next day, the fresh medium with 0, 1, 2, 4, 8, 16, 32 μ M lenvatinib were replaced (five wells per group). After 48 h of cell culture, each well was added with a total of 10 μ L CCK8 solution, and the cells in wells were incubated for 2 h. The absorbance values at 570 nm were measured, which were also utilized to represent cell viability rates in different groups. The cell viability rates were calculated = (average OD in experimental group – average OD in blank control)/(average OD in control group – average OD in blank control) \times 100 %. The results were analyzed by nonlinear regression analysis using GraphPad Prism 8.

2.17. Cellular ubiquitination assay and co-immunoprecipitation

HepG2 cells were transfected with HA-ubiquitin and the indicated constructs. After 36 h of transfection, cells were treated with MG132 (S2619, Selleckchem, Houston, USA) (25 μ M) for 8 h. The protein extraction method was same as before. For co-immunoprecipitation (co-IP), the cell lysates were centrifuged at 13,500 rpm for 20 min. The supernatant was removed and incubated with anti-Flag M2 agarose beads (SA042100, Smart-Lifesciences, Changzhou, CHINA) at 4 °C overnight. The bound beads are then washed three times with BC100 buffer (20 mM Tris-Cl, pH 7.9, 100 mM NaCl, 0.2 mM EDTA, 20 % glycerol) containing 0.2 % Triton X-100. Proteins were eluted with 3 \times Flag peptide for 4 h at 4 °C. The ubiquitinated forms of KRAS as well as the immunoprecipitated pull-down proteins were detected by Western blot using an anti-HA antibody coupled with other labeling antibodies.

2.18. Cycloheximide chase assay

HepG2 and SK-Hep1 cells were used for the cycloheximide (CHX) chase assay. CHX was dissolved in dimethyl sulfoxide (DMSO) and diluted in culture medium. HepG2 cells were seeded in 12-well plates, six of which were seeded with LZTR1 overexpression cells, the other six were seeded with control cells. SK-Hep1 cells were seeded in 12-well plates, the six of which were treated with lenvatinib (12 μ M) dissolved in DMSO, other six were treated with an equal amount of DMSO. The fresh medium with 50 μ g/ml CHX were replaced to block protein synthesis when the cells were in the logarithmic growth phase. Next, cell lysates were prepared at 0, 4, 8, 12, 20 and 28 h after CHX addition. The samples were analyzed by Western blot as described above.

2.19. Lenvatinib resistance inducible experiment

HepG2 and SK-Hep1 cells were chosen to conduct the lenvatinib resistance inducible experiments. Lenvatinib was purchased from Zhengda Tianqing Pharmaceutical Group Co., Ltd., the national medicine standard was H20213638. Lenvatinib was dissolved in DMSO and diluted to the experimental concentration in culture medium. The stock solution of lenvatinib was prepared in DMSO for 5 μ M. The HCC cells were seeded in 12-well plates, and the fresh medium with 0, 4, 8, 12, 16, 20 μ M lenvatinib were replaced when cells were in the logarithmic growth phase. Two replicate wells were evaluated for each concentration in a 12-well plate. 48 h later, 6-well cells were collected to prepare cell lysates for Western blot as described above, other 6-well cells were collected, and their RNA was extracted for RT-qPCR as described above.

2.20. Kyoto encyclopedia of genes and genomes and gene ontology analysis

The raw proteomic data of LZTR1 in HCC tissues were downloaded from the CPTAC Data Portal (<https://pdc.cancer.gov/pdc/>). According to the LZTR1 protein levels, the top 25 % (High) and bottom 25 % (Low) of HCC tissues were kept and divided into two groups. Significant differentially expressed proteins were filtered by T-test using R software. The Gene ontology (GO) and Kyoto encyclopedia of genes and genomes (KEGG) enrichment analyses (<http://www.geneontology.org/>) were conducted by the “colorspace”, “stringi”, “ggplot2”, “BiocManager” packages in R software.

2.21. Statistical analysis

Statistical analyses were performed using the statistical package of GraphPad Prism version 8. Image analyses were performed using Image J software. All data were expressed as mean \pm SD (N \geq 3). The data of relationship between clinicopathological characteristics and LZTR1 mRNA (Supplementary file 1-Fig. 1A), protein (Fig. 1D), and histological expression (Fig. 1H) was assessed using the Chi-squared test. The data of IHC staining intensity and staining score (Fig. 1I) were assessed using the Chi-squared test. The Kaplan-Meier survival analysis was used for survival analysis (Fig. 1E–F and Supplementary file 1-Fig. 1D). Bivariate correlations (Fig. 4A–C and Supplementary file 1-Fig. 1E and F) were assessed using the Pearson correlation coefficient. The data of clinicopathological characteristics (Tables 1 and 2) were assessed using the Chi-squared test. Besides, for other data, non-paired test was conducted if normality test was satisfied, and the Wilcoxon rank sum test was conducted if the normality test was not satisfied.

3. Results

3.1. The protein level of LZTR1 is aberrantly lower in HCC tissues, related to the worse outcome of HCC patients

To verify LZTR1 expression between HCC tissues and normal liver tissues, and the correlation between LZTR1 expression and prognosis in HCC patients. We downloaded the RNA-seq data (FPKM value) of LZTR1 in HCC tissues and normal liver tissues from TCGA and GTEx databases and found no significant difference in mRNA expression levels among them (Fig. 1A). As for the protein expression level, the raw proteomic data of LZTR1 in HCC from the CPTAC Data Portal were downloaded, and we further performed overall and paired differential LZTR1 protein expression analyses and observed that LZTR1 protein expression was aberrantly lower in HCC tissues compared with adjacent normal tissue, the difference was statistically significant ($P < 0.001$) (Fig. 1B–C). The clinicopathological characteristics of 159 HCC patients were downloaded from the CPTAC database and these characteristics were analyzed according to high and low expression of LZTR1 protein level. The top 25 % (High) and bottom 25 % (Low) of patients were kept, and the result was shown with a heatmap using R software. Multiple tumors were present in 17 of 40 patients from the high LZTR1 protein expression group and in 7 of 40 patients from the low LZTR1 protein expression group. The difference was statistically significant ($P <$

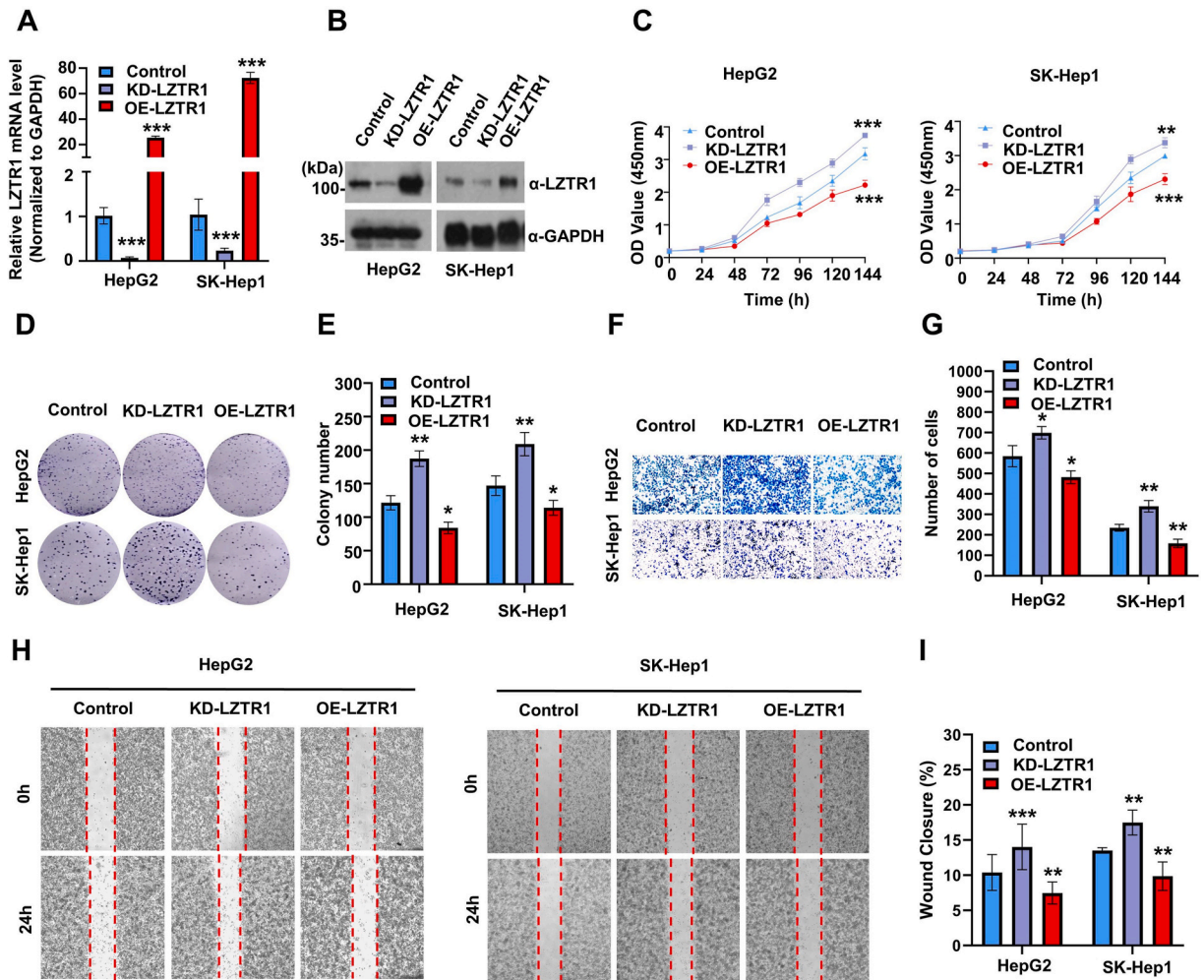


Fig. 2. LZTR1 inhibits HCC cell proliferation, migration and colony formation *in vitro*. **A** RT-qPCR was used to confirm the LZTR1 mRNA expression in HepG2 and SK-Hep1 stable expression cell lines. (KD: knockdown, OE: overexpression). Data are shown as mean \pm SD ($N \geq 3$). **B** Western blot was used to confirm the LZTR1 protein expression in HepG2 and SK-Hep1 stable expression cell lines. **C** CCK8 assay was used to observe the proliferation of HepG2 and SK-Hep1 stable expression cell lines. **D–E** Plate colony formation assay was used to determine the colony formation abilities in HepG2 and SK-Hep1 stable expression cell lines. Results of colony number were shown as column charts. **F–G** Transwell migration assay was used to discover the migration abilities in SK-Hep1 and HepG2 stable expression cell lines. Results of migrated cells number were shown as column charts. **H–I** Wound healing migration assay was used to discover the migration abilities in HepG2 and SK-Hep1 stable expression cell lines. Results of wound healing rates were shown as column charts. Asterisk represents the significant difference. * $P < 0.05$, ** $P < 0.01$, *** $P < 0.001$. All data are shown as mean \pm SD ($N \geq 3$). The original image for Fig. 2B is shown in “Supplementary file of original images”.

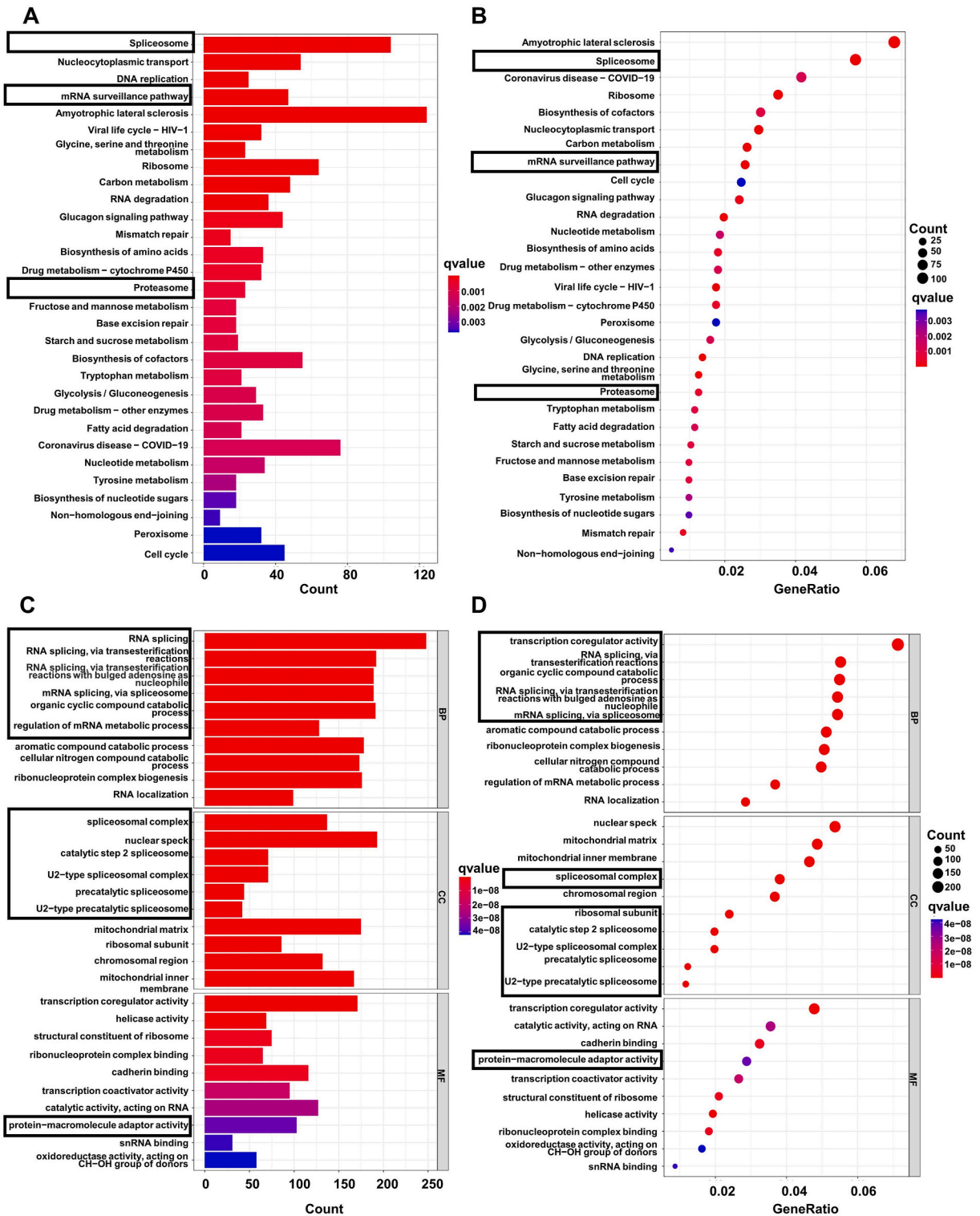
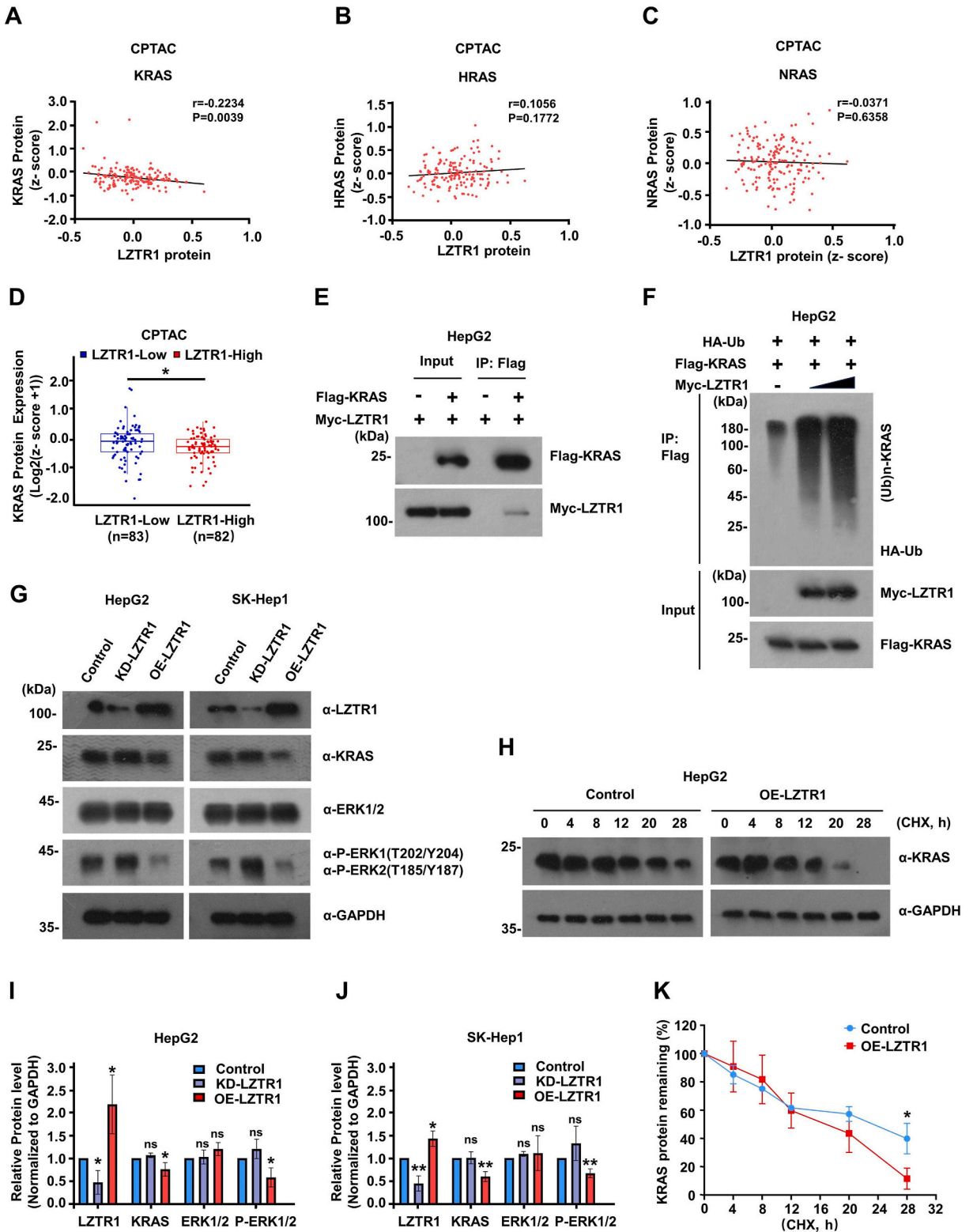


Fig. 3. KEGG and GO analysis of the differentially expressed proteins. A A barplot diagram shows the KEGG pathway enrichment analyses using R software. B A bubble diagram shows the KEGG pathway enrichment analyses using R software. C A barplot diagram shows the GO enrichment analyses using R software. D A bubble diagram shows the GO enrichment analyses using R software.



(caption on next page)

Fig. 4. LZTR1 inhibits the RAS/RAF/MEK/ERK signaling by destabilizing KRAS protein in HCC cells. **A–C** The correlation between LZTR1 protein levels and the classical Ras family members (KRAS, HRAS and NRAS) in HCC tissues from CPTAC database using R software. **D** Differential expression analysis of KRAS protein levels in LZTR1-high expressed HCC tissues and LZTR1-low expressed HCC tissues from CPTAC database using R software. **E** Co-immunoprecipitation was used to confirm the interaction between KRAS and LZTR1 in HepG2 cells. **F** Cellular ubiquitination assay was used to reveal that LZTR1 facilitates the KRAS ubiquitination modification in HepG2 cells. **G** Western blot was used to confirm the downstream proteins expression levels of RAS/RAF/MEK/ERK signaling in HepG2 and SK-Hep1 stable expression cell lines. **H** Western blot was used to confirm the degradation rates of KRAS protein in HepG2 cells. **I–J** Results of protein expression levels were shown as column charts. **K** Results of KRAS protein degradation rates were shown as the line graph. Asterisk represents the significant difference. * $P < 0.05$, ** $P < 0.01$, *** $P < 0.001$. The original images for Fig. 4E–H are shown in “Supplementary file of original images”.

0.05) (Fig. 1D). Moreover, survival analysis indicated that patients with higher LZTR1 protein expression in HCC tissues had longer overall survival times than those with lower LZTR1 protein expression ($P < 0.05$) (Fig. 1E). The patients with higher LZTR1 protein expression also had longer disease progression survival times, although this difference was not statistically significant (Fig. 1F).

We collected 7 pairs of HCC tissues and its adjacent normal tissues, and found that the tumor tissues had relatively higher LZTR1 expression at protein levels, but there was no statistical difference in mRNA levels (Supplementary file 1-Fig. 4A–C). To further confirm the expression of LZTR1 in HCC tissues, we performed IHC staining of 76 pairs of HCC tissues and adjacent normal tissues with LZTR1 antibody. Based on staining intensity, the results were divided into negative, low positive and high positive. Representative images of negative, low positive and high positive IHC staining were shown in Fig. 1G. The LZTR1 protein expression in HCC tissues (52.6 % negative, 35.5 % low positive, 11.9 % high positive) was significantly lower than that in adjacent normal tissues (15.8 % negative, 52.6 % low positive, 31.6 % high positive), of which the difference was statistically significant ($P < 0.001$) (Table 1). The patients were grouped into negative (40/76) and positive (36/76) groups according to the staining intensity of their HCC tissues. The clinicopathological characteristics were shown in a heatmap of correlations between LZTR1 expression and clinical variables (Fig. 1H and Table 2). According to the sum of staining intensity and positive cell scores, the total scores in HCC tissues were significantly lower than those in adjacent normal tissues (Fig. 1D), and the difference was statistically significant ($P < 0.001$). Microvascular invasion (MVI), a histological feature of HCC, is closely associated with aggressive biological behavior and its grade is of great importance for evaluating HCC recurrence and selecting postoperative treatment [30]. In our study, the MVI were categorized into two groups: low-risk (M0–M1) and high-risk (M2). After further analysis, we found that the positive group had a significant lower MVI grade than that of the negative group ($P < 0.05$) (Fig. 1J).

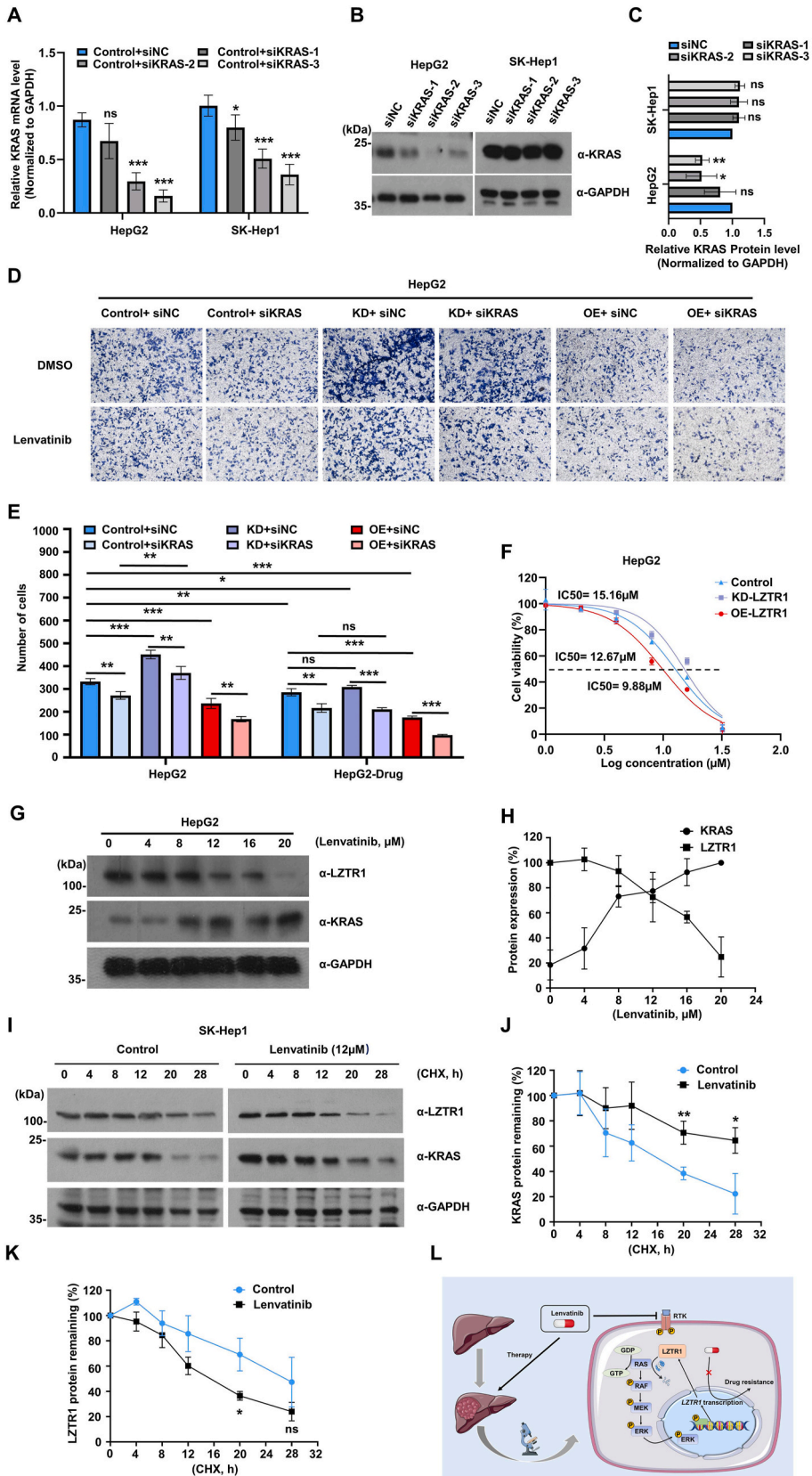
3.2. Low expression of LZTR1 facilitates HCC cell proliferation and migration in vitro

HepG2 and SK-Hep1 cells were chosen for subsequent *in vitro* assays. RT-qPCR and Western blot were used to confirm the mRNA and protein expression of LZTR1 in HepG2 and SK-Hep1 cell lines, as shown in Fig. 2A–B. Cell proliferation assay using CCK8 showed that overexpression of LZTR1 markedly inhibited HCC cell proliferation, while low expression of LZTR1 significantly promoted HCC cell proliferation (Fig. 2C). In colony formation assay, the number of average colony count with overexpression of LZTR1 was dramatically lower than that of the control group, and the cells with low expression of LZTR1 showed a stronger ability of colony formation (Fig. 2D–E). Transwell migration and wound healing migration assays were used to investigate the effect of LZTR1 on HCC cells migration. The number of cells in the transwell chamber in low expression of LZTR1 group was higher than that in the control group, while the number of cells in the transwell chamber in overexpression of LZTR1 group was less than that in the control group (Fig. 2F–G). In wound healing migration assay, scratch closure rates (%) at 24 h post-scratch were measured to assess cell migration. Compared with control group, the overexpression of LZTR1 HCC cells showed lower mobility, meanwhile low expression of LZTR1 HCC cells showed higher mobility (Fig. 2H–I). All the results showed that low expression of LZTR1 promoted HCC cells proliferation and migration *in vitro*.

3.3. KEGG and GO analysis of the differentially expressed proteins

The GO [31] and KEGG [32] are two widely used biological databases for high-level biological functions. HCC-associated bioinformatic analysis was conducted using KEGG and GO enrichment analyses. Patients whose protein expression levels of LZTR1 were in the top 25 % or bottom 25 % were considered the LZTR1-high or LZTR1-low group, respectively. The differential expression proteins screening was performed as described above, and a total of 3770 proteins were found differentially expressed, of which 1734 were upregulated ($P \leq 0.05$) and 2036 ($P \leq 0.05$) were downregulated in the LZTR1-low group as compared to LZTR1-high group. And, GO enrichment analysis and KEGG pathway enrichment analysis were performed using R software and the results were shown in barplot diagrams and bubble diagrams (Fig. 3A–D).

As mentioned above, LZTR1, as a substrate specific adaptor for the CRL3 ubiquitin ligase complex, facilitates ubiquitination and degradation of RAS GTPases [33]. As shown in the above experiments, LZTR1 was aberrantly lowly expressed in HCC tissues at protein levels and inhibited HCC cell proliferation and migration. To date, the underlying tumor-suppressor roles of LZTR1 in HCC are still unclear, and it is also unknown whether LZTR1 is involved in the ubiquitination of RAS GTPases in HCC. In the enrichment analysis results, we noticed that GO enrichment analysis included “Protein-macromolecule adaptor activity”, and KEGG enrichment analysis included “Proteasome pathway”. To further investigate its tumor suppressive role, we next designed experiments and evaluated whether LZTR1 induces RAS GTPases degradation.



(caption on next page)

Fig. 5. LZTR1 inhibits HCC cell migration by inhibiting the RAS/RAF/MEK/ERK signaling *in vitro*. Low expression of LZTR1 is associated with resistance to lenvatinib in HCC cell lines. A RT-qPCR was used to confirm the efficiency of siKRAS knockdown in HepG2 and SK-Hep1 cell lines. Data were shown as mean \pm SD ($N \geq 3$). **B–C** Western blot was used to confirm the siKRAS knockdown efficiency in HepG2 and SK-Hep1 stable expression cell lines. The results of protein expression levels were shown as a column chart. **D–E** Transwell migration assay was used to determine the migration abilities in HepG2 stable expression cell lines with KRAS knockdown and in HepG2 stable expression cell lines exposed to lenvatinib (4 μ M). Results of migrated cells number were shown as column charts. **F** IC50 assay was used to detect the lenvatinib's inhibitory efficacy in HCC stable expression cell lines. **G–H** Western blot was used to indicated the LZTR1 and KRAS protein expression in lenvatinib resistance HCC cells. Results of protein degradation rates were shown as the line graph. **I–K** Western blot was used to confirm the degradation rates of KRAS and LZTR1 protein in SK-Hep1 cells exposure to lenvatinib. Results of protein degradation rates were shown as the line graphs. **L** Graphical Abstract: Lenvatinib inhibits LZTR1 transcription, which excessively activates the RAS/RAF/MEK/ERK signaling to entitle HCC cell to acquire drug resistance. Asterisk represents the significant difference. * $P < 0.05$, ** $P < 0.01$, *** $P < 0.001$. Data are shown as mean \pm SD ($N \geq 3$). The original images for Fig. 5B–G and I are shown in “Supplementary file of original images”.

3.4. LZTR1 destabilizes RAS protein in HCC cell lines

By analyzing the database of CPTAC, the correlations between three most important members of RAS GTPases family (KRAS, NRAS, HRAS) and LZTR1 were performed by Pearson correlation analysis, the results were shown in Fig. 4A–C. In addition, the correlation between LZTR1 and the key protein molecules, including RAF1, MEK1, MEK2, ERK1, and ERK2, and the key phosphorylated protein molecules, including P-MEK1, P-MEK2, P-ERK1 and P-ERK2 were also shown in Supplementary file 1-Fig. 1E and F. At the protein levels, only KRAS was negatively correlated with LZTR1 expression in HCC tissues (Fig. 4A). Furthermore, the 165 tumor tissues were divided into two groups based on the median levels of LZTR1 protein expression. We found that KRAS protein expression levels in the LZTR1 high expression group were significantly lower than that in the LZTR1 low expression group, and the results were presented as the box-plot (Fig. 4D). Previous studies have demonstrated that LZTR1 can induce KRAS ubiquitination and degradation [26,33], and this effect was also confirmed in pancreatic cancer [28] and melanoma [29]. Further, through the co-IP and cellular ubiquitination assay, we showed that LZTR1 interacted with KRAS (Fig. 4E), and induced its ubiquitination and degradation (Fig. 4F). Therefore, we hypothesized that LZTR1 destabilizes KRAS protein by ubiquitination and degradation to inhibit the RAS/RAF/MEK/ERK signaling, thereby inhibiting HCC progression.

Western blot was used to detect the downstream proteins expression levels of RAS/RAF/MEK/ERK signaling, including KRAS, ERK1/2 and P-ERK1/2. In LZTR1-overexpressed HepG2 and SK-Hep1 cells, we found that the KRAS and P-ERK1/2 protein levels were decreased compared with the control or LZTR1-knockdown cells (Fig. 4G and I–J). In addition, the degradation rate of KRAS was determined using CHX chase assay, and the results showed that LZTR1 accelerated the KRAS degradation in HCC cells (Fig. 4H and K).

3.5. Low expression of LZTR1 facilitates HCC cell proliferation and migration by activating the RAS/RAF/MEK/ERK signaling

Frequent activation of RAS/RAF/MEK/ERK signaling has been observed in HCC patients [18]. Elevated RAS expression is highly correlated with an unfavorable prognosis of HCC patients [34]. In our study, we found that LZTR1 destabilized KRAS in HCC cells (Fig. 4G–K). To date, it is unclear whether low expression of LZTR1 promotes HCC progression *via* maintaining KRAS protein stability.

The HepG2 and SK-Hep1 stable expression cells were transfected with short interfering RNA (siRNA) targeting KRAS (siKRAS) or control siRNA (siNC). The knockdown efficiency in HCC and SK-Hep1 cells was verified by RT-qPCR and Western blot (Fig. 5A–C). In the results, knockdown of KRAS protein was observed in HepG2 cells treated with siKRAS, else, siKRAS-3 exhibited the best inhibitory effect. However, no obvious differences were observed in SK-Hep1 cells by Western blot, meanwhile. Therefore, the siKRAS-3 was chosen for following experiments in HepG2 cells. Notably, in transwell migration assay, we found that KRAS knockdown reduced the migration ability of HCC cells and counteracted the cell migration enhanced by LZTR1 knockdown (Fig. 5D–E). The endogenous LZTR1 expression levels were explored among HCC cell lines, and HepG2 and SK-Hep1 were identified to show the relatively higher endogenous LZTR1 expression (Supplementary file 1-Fig. 5A and B).

3.6. Low expression of LZTR1 results in resistance to lenvatinib in HCC cell lines

Lenvatinib, a multi-targeted kinase inhibitor, is a first-line treatment for advanced HCC and entitled an improved therapeutic effect in HCC [35]. However, drug resistance inevitably emerges with progress in treatment [36]. Previous study has demonstrated that upregulating the RAS/RAF/MEK/ERK signaling led to the lenvatinib resistance [19], but the underlying mechanisms were still unclear. IC50 assays were conducted, and it was found that low expression of LZTR1 upregulated the lenvatinib IC50 (15.16 μ M vs 12.67 μ M), and overexpression of LZTR1 downregulated the lenvatinib IC50 in HepG2 cells (9.88 μ M vs 12.67 μ M), the results were shown in Fig. 5F. In addition, we found that LZTR1 protein was downregulated and KRAS protein was upregulated after HCC cells exposure to lenvatinib for 48 h (Fig. 5G–H). Besides, the mRNA levels of LZTR1 and KRAS were decreased as the lenvatinib concentration increased (Supplementary file 1-Fig. 2D–E). We found that the LZTR1 protein expression decreased and the KRAS protein expression increased with the increasing lenvatinib concentrations in HCC cells (Supplementary file 1-Fig. 2A and B). In addition, the CHX chase assay was used to determine the degradation rates of KRAS and LZTR1 upon exposure to lenvatinib (12 μ M). The results showed that lenvatinib exposure (12 μ M) accelerated LZTR1 degradation but delayed KRAS degradation in HCC cells (Fig. 5I–K). *In vitro* experiments, transwell assays showed that blocking LZTR1-mediated KRAS degradation induced lenvatinib resistance in HepG2 cells exposed to lenvatinib exposure (4 μ M) (Fig. 5D).

4. Discussion

LZTR1, a substrate-specific adaptor for the CRL3 ubiquitin ligase complex, has been discovered involved in ubiquitination and degradation of RAS GTPase protein [26,33] and inhibits the progression of pancreatic cancer [28] and melanoma [29]. Nevertheless, there exists no study of LZTR1-associated roles in HCC progression. Herein, we are the first study to find that LZTR1 is aberrantly expressed at low levels in HCC and induces activation of the RAS/RAF/MEK/ERK signaling, thus promoting HCC cell proliferation and migration. Based on our experimental results, we reasonably speculated that low expression of LZTR1 may contribute to KRAS stabilization and activate the RAS/RAF/MEK/ERK signaling, thus inducing lenvatinib resistance, which also suggests the great potential of LZTR1 as a promising therapeutic target to reverse lenvatinib resistance.

Interestingly, at the *LZTR1* mRNA level, no significant difference was found between HCC tissue and adjacent normal tissues in biological databases (Fig. 1A). Besides, in TCGA database, it was detected that high *LZTR1* mRNA expression correlated with poor prognosis, which was diametrically contrary to the result analyzed based on protein levels (Supplementary file 1-Fig. 1A–D). This difference may be explained by proteomic and transcriptomic analyses in the future. Besides, little is known about the PTMs of LZTR1 protein, nowadays. Palanivel et al. firstly revealed that glycogen synthase kinase-3 (GSK-3) activated LZTR1 through phosphorylation without affecting its protein levels, and the activated LZTR1 in turn promoted KRAS degradation, inhibiting the RAS/RAF/MEK/ERK signaling to suppress pancreatic cancer progression [28]. Ambivalent results analyzed by bioinformatics were detected between the *LZTR1* mRNA and protein levels in HCC tissues. Therefore, conjectures are proposed that whether there possibly exist aberrant LZTR1 degradation mechanisms in HCC progression.

RNA splicing is a critical process in the transformation from pre-mRNA to mature mRNA through intron removal, which is involved in regulating gene expression, mRNA decay, protein translation, and biological function [37]. A large number of studies have revealed that aberrant splicing has widely been implicated in tumorigenesis [38,39] and anti-tumor drug resistance [40,41], and deemed a hallmark of cancer [42]. RNA splicing is mainly regulated by the spliceosome and splicing factors (SFs), its aberrant regulation has been found in a series of human tumors, which can be caused by SFs-coding gene mutations [43,44]. Studies have found that the mutation of *ZRSR2*, one SF-coding gene, leads to the aberrant splicing and intron retention of *LZTR1*, which severely disrupts *LZTR1* mRNA stability, inhibits protein translation, and then promotes RAS protein accumulation, inducing BCR/ABL-TKI (imatinib) resistance in leukemia cells [45]. In addition, another study found that the abnormal *LZTR1* intron retention existence in all types of tumors, including HCC [45]. Consistently, the “spliceosome”, and “mRNA surveillance pathway” were enriched in KEGG analysis, and the “RNA splicing”, “mRNA splicing, via spliceosome”, “regulation of mRNA metabolic process”, “spliceosomal complex”, “U2-type spliceosome”, “pre-catalytic spliceosome” were enriched in GO analysis (Fig. 3). Therefore, we speculate the abnormal splicing of *LZTR1* may destroy mRNA stability and thus inhibits protein translation in HCC, thereby suppressing RAS protein degradation and activating the RAS/RAF/MEK/ERK signaling contributing to HCC progression and lenvatinib resistance occurrence. Besides, our preliminary experimental results in lenvatinib resistance inducible HCC cells also fitted well with this notion. The decreased mRNA and protein levels of LZTR1 upon exposure to lenvatinib were detected *in vitro* (Fig. 5G, Supplementary file 1-Fig. 2A–E), and more convinced evidence should be collected *in vivo* in the future.

In addition, genetic mutation may alter the function of E3 ligase adaptor, such as *SPOP*, exhibiting the loss of function in PCa [46]. Nowadays, *LZTR1* mutations have been identified in HCC, but little is known about the effects of LZTR1 mutations on occurrence and progression of HCC, as well as drug resistance [47]. To further study the HCC-associated LZTR1 mutation by knock-in mice model may address these issues. Besides, the structure of LZTR1 should also be confirmed in the future for a better search for its agonist to enhance its tumor suppressive role in HCC.

Finally, there are still deficiencies in our study that remain to be improved in the future. Herein, we utilized bioinformatics analyses, molecular biological tests, *in vitro* experiments, and human histopathology evaluations to explore the tumor suppressive role of LZTR1 in HCC, but there is still a lack of *in vivo* experiments to confirm this result. Additionally, we mainly focused our research on LZTR1-mediated ubiquitination and degradation of RAS signaling, but unveiled the underlying mechanism involved in regulating LZTR1 expression levels and biological function through alternative splicing, nuclear transport, protein translation, and PTM, etc.

Funding

This research was funded by Natural Science Foundation of Ningbo (Grant No. 2021J065 and 2022J230), Youth Science and Technology Innovation Leader of Ningbo (Grant No. 2023QL052), Ningbo Health Technology Project (Grant No. 2022Y13), The National Natural Science Foundation of China (Grant No. 32270821), The National Natural Science Foundation of China (Grant No LY24C050001 and LTGY24H160004), The Ningbo University Student Research and Innovation Program (Grant No. 2023-292, 2024-017, 2024-025 and 2024-034) and The K.C. Wong Magna Fund in Ningbo University.

Data availability statement

The data generated in our study are not deposited into a publicly available repository, which are available from the first author on reasonable request.

Ethics approval

All human samples were obtained after the patients' informed consent. This study was reviewed and approved by the ethics

committee of Health Science Center of Ningbo University with the approval number: NBU-2021-121, dated July 10, 2021.

CRedit authorship contribution statement

Ganghui Ye: Writing – review & editing, Writing – original draft, Validation, Supervision, Investigation, Formal analysis, Data curation. **Jie Wang:** Funding acquisition, Formal analysis. **Jingyi Xia:** Investigation, Data curation. **Chenlu Zhu:** Investigation, Data curation. **Chaoyu Gu:** Investigation, Data curation. **Xinming Li:** Investigation, Data curation. **Jingyun Li:** Resources, Funding acquisition. **Meng Ye:** Writing – review & editing. **Xiaofeng Jin:** Writing – review & editing, Writing – original draft, Validation, Resources, Investigation, Funding acquisition.

Declaration of competing interest

The authors declare the following financial interests/personal relationships which may be considered as potential competing interests: Xiaia reports equipment, drugs, or supplies and statistical analysis were provided by Ningbo Clinicopathological Diagnosis Centre. If there are other authors, they declare that they have no known competing financial interests or personal relationships that could have appeared to influence the work reported in this paper.

Acknowledgements

We would like to be very grateful to Lu Li from the Ningbo Clinicopathological Diagnosis Center, Gun Chen from the Departments of Pathology, Yinzhou People's Hospital of Medical School for the immunohistochemical staining analyses.

Appendix A. Supplementary data

Supplementary data to this article can be found online at <https://doi.org/10.1016/j.heliyon.2024.e32855>.

References

- [1] H. Sung, J. Ferlay, R.L. Siegel, M. Laversanne, I. Soerjomataram, A. Jemal, F. Bray, Global cancer statistics 2020: GLOBOCAN estimates of incidence and mortality worldwide for 36 cancers in 185 countries, *CA A Cancer J. Clin.* 71 (3) (2021) 209–249.
- [2] R. Zheng, S. Zhang, H. Zeng, S. Wang, K. Sun, R. Chen, L. Li, W. Wei, J. He, Cancer incidence and mortality in China, 2016, *Journal of the National Cancer Center* (2022).
- [3] A. Huang, X.R. Yang, W.Y. Chung, A.R. Dennison, J. Zhou, Targeted therapy for hepatocellular carcinoma, *Signal Transduct. Targeted Ther.* 5 (1) (2020) 146.
- [4] E. Mizukoshi, S. Kaneko, Immune cell therapy for hepatocellular carcinoma, *J. Hematol. Oncol.* 12 (1) (2019) 52.
- [5] H.C. Lee, M. Kim, J.R. Wands, Wnt/Frizzled signaling in hepatocellular carcinoma, *Front. Biosci.* 11 (2006) 1901–1915.
- [6] M.S. Matter, T. Decaens, J.B. Andersen, S.S. Thorgeirsson, Targeting the mTOR pathway in hepatocellular carcinoma: current state and future trends, *J. Hepatol.* 60 (4) (2014) 855–865.
- [7] H. Moon, S.W. Ro, MAPK/ERK signaling pathway in hepatocellular carcinoma, *Cancers* 13 (12) (2021).
- [8] C. Neuzillet, A. Tijeras-Raballand, L. de Mestier, J. Cros, S. Faivre, E. Raymond, MEK in cancer and cancer therapy, *Pharmacol. Ther.* 141 (2) (2014) 160–171.
- [9] X. Yang, Y.T. Zheng, W. Rong, Sevoflurane induces apoptosis and inhibits the growth and motility of colon cancer in vitro and in vivo via inactivating Ras/Raf/MEK/ERK signaling, *Life Sci.* 239 (2019) 116916.
- [10] S.M. Akula, S.L. Abrams, L.S. Steelman, M.R. Emma, G. Augello, A. Cusimano, A. Azzolina, G. Montalto, M. Cervello, J.A. McCubrey, RAS/RAF/MEK/ERK, PI3K/PTEN/AKT/mTORC1 and TP53 pathways and regulatory miRNAs as therapeutic targets in hepatocellular carcinoma, *Expert Opin. Ther. Targets* 23 (11) (2019) 915–929.
- [11] L.S. Steelman, R.A. Franklin, S.L. Abrams, W. Chappell, C.R. Kempf, J. Basecke, F. Stivala, M. Donia, P. Fagone, F. Nicoletti, M. Libra, P. Ruvolo, V. Ruvolo, C. Evangelisti, A.M. Martelli, J.A. McCubrey, Roles of the Ras/Raf/MEK/ERK pathway in leukemia therapy, *Leukemia* 25 (7) (2011) 1080–1094.
- [12] A.X. Wang, X.Y. Qi, Targeting RAS/RAF/MEK/ERK signaling in metastatic melanoma, *IUBMB Life* 65 (9) (2013) 748–758.
- [13] P.J. Roberts, C.J. Der, Targeting the Raf-MEK-ERK mitogen-activated protein kinase cascade for the treatment of cancer, *Oncogene* 26 (22) (2007) 3291–3310.
- [14] S. Garces, C.C. Yin, K.P. Patel, J.D. Khoury, J.T. Manning Jr., S. Li, J. Xu, S. Pina-Oviedo, M.R. Johnson, S. González, M. Molgó, R. Ruiz-Cordero, L.J. Medeiros, Focal Rosai-Dorfman disease coexisting with lymphoma in the same anatomic site: a localized histiocytic proliferation associated with MAPK/ERK pathway activation, *Mod. Pathol.* 32 (1) (2019) 16–26.
- [15] Y.J. Guo, W.W. Pan, S.B. Liu, Z.F. Shen, Y. Xu, L.L. Hu, ERK/MAPK signalling pathway and tumorigenesis, *Exp. Ther. Med.* 19 (3) (2020) 1997–2007.
- [16] S. Schubert, K. Shannon, G. Bollag, Hyperactive Ras in developmental disorders and cancer, *Nat. Rev. Cancer* 7 (4) (2007) 295–308.
- [17] Y. Pylyayeva-Gupta, E. Grabocka, D. Bar-Sagi, RAS oncogenes: weaving a tumorigenic web, *Nat. Rev. Cancer* 11 (11) (2011) 761–774.
- [18] L. Li, G.D. Zhao, Z. Shi, L.L. Qi, L.Y. Zhou, Z.X. Fu, The Ras/Raf/MEK/ERK signaling pathway and its role in the occurrence and development of HCC, *Oncol. Lett.* 12 (5) (2016) 3045–3050.
- [19] Z. Zhao, D. Zhang, F. Wu, J. Tu, J. Song, M. Xu, J. Ji, Sophoridine suppresses lenvatinib-resistant hepatocellular carcinoma growth by inhibiting RAS/MEK/ERK axis via decreasing VEGFR2 expression, *J. Cell Mol. Med.* 25 (1) (2021) 549–560.
- [20] A. Taketomi, K. Shirabe, J. Muto, S. Yoshiya, T. Motomura, Y. Mano, T. Ikegami, T. Yoshizumi, K. Sugio, Y. Maehara, A rare point mutation in the Ras oncogene in hepatocellular carcinoma, *Surg. Today* 43 (3) (2013) 289–292.
- [21] R. Yau, M. Rape, The increasing complexity of the ubiquitin code, *Nat. Cell Biol.* 18 (6) (2016) 579–586.
- [22] D. Hoeller, I. Dikic, Targeting the ubiquitin system in cancer therapy, *Nature* 458 (7237) (2009) 438–444.
- [23] Z. Yu, H. Li, J. Zhu, H. Wang, X. Jin, The roles of E3 ligases in Hepatocellular carcinoma, *Am. J. Cancer Res.* 12 (3) (2022) 1179–1214.
- [24] T.G. Nacak, K. Leptien, D. Fellner, H.G. Augustin, J. Kroll, The BTB-kelch protein LZTR-1 is a novel Golgi protein that is degraded upon induction of apoptosis, *J. Biol. Chem.* 281 (8) (2006) 5065–5071.
- [25] H. Zhang, X. Cao, J. Wang, Q. Li, Y. Zhao, X. Jin, LZTR1: a promising adaptor of the CUL3 family, *Oncol. Lett.* 22 (1) (2021) 564.

- [26] J.W. Bigenzahn, G.M. Collu, F. Kartnig, M. Pieraks, G.I. Vladimer, L.X. Heinz, V. Sedlyarov, F. Schischlik, A. Fauster, M. Rebsamen, K. Parapatics, V.A. Blomen, A.C. Muller, G.E. Winter, R. Kralovics, T.R. Brummelkamp, M. Mlodzik, G. Superti-Furga, LZTR1 is a regulator of RAS ubiquitination and signaling, *Science* 362 (6419) (2018) 1171–1177.
- [27] M. Steklov, S. Pandolfi, M.F. Baietti, A. Batiuk, P. Carai, P. Najm, M. Zhang, H. Jang, F. Renzi, Y. Cai, L. Abbasi Asbagh, T. Pastor, M. De Troyer, M. Simicek, E. Radaelli, H. Brems, E. Legius, J. Tavernier, K. Gevaert, F. Impens, L. Messiaen, R. Nussinov, S. Heymans, S. Eyckerman, A.A. Sablina, Mutations in LZTR1 drive human disease by dysregulating RAS ubiquitination, *Science* 362 (6419) (2018) 1177–1182.
- [28] C. Palanivel, N. Chaudhary, P. Seshacharyulu, J.L. Cox, Y. Yan, S.K. Batra, M.M. Ouellette, The GSK3 kinase and LZTR1 protein regulate the stability of Ras family proteins and the proliferation of pancreatic cancer cells, *Neoplasia* 25 (2022) 28–40.
- [29] F. Farshidfar, K. Rhrissorrakrai, C. Levovitz, C. Peng, J. Knight, A. Bacchiocchi, J. Su, M. Yin, M. Sznol, S. Ariyan, J. Clune, K. Olino, L. Parida, J. Nikolaus, M. Zhang, S. Zhao, Y. Wang, G. Huang, M. Wan, X. Li, J. Cao, Q. Yan, X. Chen, A.M. Newman, R. Halaban, Integrative molecular and clinical profiling of acral melanoma links focal amplification of 22q11.21 to metastasis, *Nat. Commun.* 13 (1) (2022) 898.
- [30] M. Rodriguez-Peralvarez, T.V. Luong, L. Andreana, T. Meyer, A.P. Dhillon, A.K. Burroughs, A systematic review of microvascular invasion in hepatocellular carcinoma: diagnostic and prognostic variability, *Ann. Surg. Oncol.* 20 (1) (2013) 325–339.
- [31] G.O. Consortium, The Gene Ontology in 2010: extensions and refinements, *Nucleic Acids Res.* 38 (Database issue) (2010) D331–D335.
- [32] K. Nishida, K. Ono, S. Kanaya, K. Takahashi, KEGGscape: a Cytoscape app for pathway data integration, *F1000Research* 3 (2014) 144.
- [33] T. Abe, I. Umeki, S.I. Kanno, S.I. Inoue, T. Niihori, Y. Aoki, LZTR1 facilitates polyubiquitination and degradation of RAS-GTPases, *Cell Death Differ.* 27 (3) (2020) 1023–1035.
- [34] L. Chen, Y. Shi, C.Y. Jiang, L.X. Wei, Y.L. Wang, G.H. Dai, Expression and prognostic role of pan-Ras, Raf-1, pMEK1 and pERK1/2 in patients with hepatocellular carcinoma, *Eur. J. Surg. Oncol. : the journal of the European Society of Surgical Oncology and the British Association of Surgical Oncology* 37 (6) (2011) 513–520.
- [35] M. Kudo, R.S. Finn, S. Qin, K.H. Han, K. Ikeda, F. Piscaglia, A. Baron, J.W. Park, G. Han, J. Jassem, J.F. Blanc, A. Vogel, D. Komov, T.R.J. Evans, C. Lopez, C. Dutcus, M. Guo, K. Saito, S. Kraljevic, T. Tamai, M. Ren, A.L. Cheng, Lenvatinib versus sorafenib in first-line treatment of patients with unresectable hepatocellular carcinoma: a randomised phase 3 non-inferiority trial, *Lancet (London, England)* 391 (10126) (2018) 1163–1173.
- [36] M. Reig, J. Bruix, Lenvatinib: can a non-inferiority trial change clinical practice? *Lancet (London, England)* 391 (10126) (2018) 1123–1124.
- [37] A.G. Matera, Z. Wang, A day in the life of the spliceosome, *Nat. Rev. Mol. Cell Biol.* 15 (2) (2014) 108–121.
- [38] A. Kahles, K.V. Lehmann, N.C. Toussaint, M. Hüser, S.G. Stark, T. Sachsenberg, O. Stegle, O. Kohlbacher, C. Sander, G. Rätsch, Comprehensive analysis of alternative splicing across tumors from 8,705 patients, *Cancer Cell* 34 (2) (2018) 211–224.e6.
- [39] H. Dvinge, E. Kim, O. Abdel-Wahab, R.K. Bradley, RNA splicing factors as oncoproteins and tumour suppressors, *Nat. Rev. Cancer* 16 (7) (2016) 413–430.
- [40] K.P. Ng, A.M. Hillmer, C.T. Chuah, W.C. Juan, T.K. Ko, A.S. Teo, P.N. Ariyaratne, N. Takahashi, K. Sawada, Y. Fei, S. Soh, W.H. Lee, J.W. Huang, J.C. Allen Jr., X. Y. Woo, N. Nagarajan, V. Kumar, A. Thalamuthu, W.T. Poh, A.L. Ang, H.T. Mya, G.F. How, L.Y. Yang, L.P. Koh, B. Chowbay, C.T. Chang, V.S. Nadarajan, W. J. Chng, H. Than, L.C. Lim, Y.T. Goh, S. Zhang, D. Poh, P. Tan, J.E. Seet, M.K. Ang, N.M. Chau, Q.S. Ng, D.S. Tan, M. Soda, K. Isobe, M.M. Nöthen, T.Y. Wong, A. Shahab, X. Ruan, V. Cacheux-Rataboul, W.K. Sung, E.H. Tan, Y. Yatabe, H. Mano, R.A. Soo, T.M. Chin, W.T. Lim, Y. Ruan, S.T. Ong, A common BIM deletion polymorphism mediates intrinsic resistance and inferior responses to tyrosine kinase inhibitors in cancer, *Nat. Med.* 18 (4) (2012) 521–528.
- [41] A. Alajati, N. Sausgruber, N. Aceto, S. Duss, S. Sarret, H. Voshol, D. Bonenfant, M. Bentires-Alj, Mammary tumor formation and metastasis evoked by a HER2 splice variant, *Cancer Res.* 73 (17) (2013) 5320–5327.
- [42] R.K. Bradley, O. Anczuków, RNA splicing dysregulation and the hallmarks of cancer, *Nat. Rev. Cancer* 23 (3) (2023) 135–155.
- [43] A. Pellagatti, R.N. Armstrong, V. Steeples, E. Sharma, E. Repapi, S. Singh, A. Sanchi, A. Radujkovic, P. Horn, H. Dolatshad, S. Roy, J. Broxholme, H. Lockstone, S. Taylor, A. Giagounidis, P. Vyas, A. Schuh, A. Hamblin, E. Papaemmanuil, S. Killick, L. Malcovati, M.L. Hennrich, A.C. Gavin, A.D. Ho, T. Luft, E. Hellström-Lindberg, M. Cazzola, C.W.J. Smith, S. Smith, J. Boulton, Impact of spliceosome mutations on RNA splicing in myelodysplasia: dysregulated genes/pathways and clinical associations, *Blood* 132 (12) (2018) 1225–1240.
- [44] J.W. Harbour, E.D. Roberson, H. Anbunathan, M.D. Onken, L.A. Worley, A.M. Bowcock, Recurrent mutations at codon 625 of the splicing factor SF3B1 in uveal melanoma, *Nat. Genet.* 45 (2) (2013) 133–135.
- [45] D. Inoue, J.T. Polaski, J. Taylor, P. Castel, S. Chen, S. Kobayashi, S.J. Hogg, Y. Hayashi, J.M.B. Pineda, E. El Marabti, C. Erickson, K. Knorr, M. Fukumoto, H. Yamazaki, A. Tanaka, C. Fukui, S.X. Lu, B.H. Durham, B. Liu, E. Wang, S. Mehta, D. Zakheim, R. Garippa, A. Penson, G.L. Chew, F. McCormick, R.K. Bradley, O. Abdel-Wahab, Minor intron retention drives clonal hematopoietic disorders and diverse cancer predisposition, *Nat. Genet.* 53 (5) (2021) 707–718.
- [46] H. Zhang, X. Jin, H. Huang, Dereglulation of SPOP in cancer, *Cancer Res.* 83 (4) (2023) 489–499.
- [47] Comprehensive and integrative genomic characterization of hepatocellular carcinoma, *Cell* 169 (7) (2017) 1327–1341.